

Gate voltage controlled thermoelectric figure of merit in three-dimensional topological insulator nanowires

Ning-Xuan Yang,^{1,2} Yan-Feng Zhou,^{1,2} Peng Lv,^{1,2} and Qing-Feng Sun^{1,2,3,*}

¹*International Center for Quantum Materials, School of Physics, Peking University, Beijing 100871, China*

²*Collaborative Innovation Center of Quantum Matter, Beijing 100871, China*

³*CAS Center for Excellence in Topological Quantum Computation, University of Chinese Academy of Sciences, Beijing 100190, China*

(Dated: March 29, 2018)

The thermoelectric properties of the surface states in three-dimensional topological insulator nanowires are studied. The Seebeck coefficients S_c and the dimensionless thermoelectrical figure of merit ZT are obtained by using the tight-binding Hamiltonian combining with the nonequilibrium Green's function method. They are strongly dependent on the gate voltage and the longitudinal and perpendicular magnetic fields. By changing the gate voltage or magnetic fields, the values of S_c and ZT can be easily controlled. At the zero magnetic fields and zero gate voltage, or at the large perpendicular magnetic field and nonzero gate voltage, ZT has the large value. Owing to the electron-hole symmetry, S_c is an odd function of the Fermi energy while ZT is an even function regardless of the magnetic fields. S_c and ZT show peaks when the quantized transmission coefficient jumps from one plateau to another. The highest peak appears while the Fermi energy is near the Dirac point. At the zero perpendicular magnetic field and zero gate voltage, the height of n th peak of S_c is $\frac{k_B}{e} \ln 2 / (|n| + 1/2)$ and $\frac{k_B}{e} \ln 2 / |n|$ for the longitudinal magnetic flux $\phi_{\parallel} = 0$ and π , respectively. Finally, we also study the effect of disorder and find that S_c and ZT are robust against disorder. In particular, the large value of ZT can survive even if at the strong disorder. These characteristics (that ZT has the large value, is easily regulated, and is robust against the disorder) are very beneficial for the application of the thermoelectricity.

PACS numbers:

I. INTRODUCTION

In recent years, the discovery of the three-dimensional (3D) topological insulators (TIs) has opened up a new field for the condensed matter physics, which is also one of the most important advances in material science.¹⁻³ TIs have attracted wide attention because of the exotic physical properties and potential huge applications in spintronics.⁴⁻⁸ TIs are characterized by the insulating bulk states and nontrivial conducting surface state, which is topologically protected by time-reversal symmetry. The time reversal invariant disorders can not cause the backscattering and can not open the gap on the surface states. The surface states, which present an odd number of gapless Dirac cones, are featured by the unique Dirac-like linear dispersion with the spin-momentum locked helical properties.⁹⁻¹² Moreover, for a TI nanowire, a gap opened in the surface states results from the π Berry phase obtained by the 2π rotation of the spin around the nanowire.¹³⁻¹⁵ However, by threading a magnetic flux $\phi_0/2 = h/2e$ paralleling the wire, an extra Aharonov-Bohm phase cancels the π Berry phase and closes the gap, i.e. wormhole effect.¹⁶⁻²⁰

The materials used to make thermoelectric generators or thermoelectric refrigerators are called thermoelectric materials, which can directly convert the thermal energy into the electrical energy each other. Thermoelectric materials have wide application prospects in thermoelectric power generation and thermoelectric refrigeration. Using thermoelectric materials to generate elec-

tricity and refrigeration will effectively solve the problem of energy sustainable utilization. TIs share similar material properties, such as heavy elements, narrow band gaps and quantum localization effect, with thermoelectric materials. Many TIs (like Bi_2Te_3 , Sb_2Te_3 and $\text{Bi}_x\text{Sb}_{1-x}$) are considered as excellent materials for thermoelectric conversion.²¹⁻²³ The new physical properties of TIs nanomaterials bring new breakthroughs to the research of thermoelectric materials and provide new opportunities for the development of thermoelectric technology. Therefore, it is very important and necessary to find high-efficiency thermoelectric materials. The conversion efficiency of thermoelectric materials depends on the dimensionless thermoelectrical figure of merit ZT . ZT is defined as $ZT = \sigma S_c^2 \mathcal{T} / \kappa$, where σ is the electric conductivity, S_c is the Seebeck coefficient, and \mathcal{T} is the operating temperature of the device, and the thermal conductivity κ is the sum of the electric thermal conductivity and lattice-thermal conductivity.²¹⁻²⁶ The higher ZT value of thermoelectric material, the better its performance. There are two ways to raise the ZT value. One is to increase the thermopower S_c and electrical conductivity. The large thermopower S_c can convert the temperature difference to the voltage at both ends of the material more effectively. The other is to reduce the thermal conductivity to minimize the energy loss induced by heat diffusion and Joule heating. However, due to the restriction of the Mott relation²⁷ and the Wiedemann-Franz law,²⁸ a high thermopower S_c leads to a low electrical conductance, and a high electrical conductivity in a material also implies a high thermal conductivity. These

three parameters need to be optimized to maximize the ZT value. The study of thermoelectric transport characteristics would be helpful in improving the conversion efficiency between the electrical energies and the thermal energies.^{21–24,26}

Generally, we consider the thermoelectric power, also called Seebeck coefficient which measures the magnitude of the longitudinal current induced by a longitudinal thermal gradient in the Seebeck effect. The thermoelectric power derived from the balance between the electric and thermal forces acting on the charge carrier, is more sensitive to the details of the density of states than the electronic conductance.^{25,27,29–32} Therefore, the thermoelectric power is more helpful to understand the particle-hole asymmetry of TIs. The thermoelectric power can clarify the details of the electronic structure of the ambipolar nature for the TI nanowires more clearly than the detection of conductance alone. Although the Seebeck effect and the Peltier effect provide a theoretical principle for the application of thermoelectric energy conversion and thermoelectric refrigeration,^{26,33} the classical Mott relation and the Wiedemann-Franz law may not be established due to the quantum behavior in nanostructured materials. Therefore, the study of thermoelectric power may inspire new ideas in the design of quantum thermoelectric devices.³⁴

In 1993, Hicks and Dresselhaus³⁵ found that ZT value increases swiftly as the dimensions decrease and strongly depends on the wire width. Hicks and Dresselhaus proposed the idea of using low-dimensional structural materials to obtain high ZT . Then more and more research groups begin to pay attention to the thermoelectric transport properties in nanostructure materials.^{36–45} Especially in recent years, with the development of the low-temperature measurement technology and the improvement of the microfabrication technology, the thermoelectric measurement in low-dimensional samples has become feasible at low temperature, and various groups were able to fabricate nanostructures and measure their thermoelectric properties at low temperature.^{36,40,43,44} In addition, the charge carrier density in nanostructured materials can easily be tuned globally or locally by varying the magnetic field or the applied gate voltage. Due to the thermoelectric effect being sensitive to the changes of carrier density, the S_c and ZT of thermoelectric materials can be controlled by applying in different directions of the magnetic field and changing the gate voltage, which opens up a broad way to find high-efficiency thermoelectric materials.²⁴

In this paper, we carry out a theoretical study of the thermoelectric properties of 3D TI nanowires under the longitudinal and perpendicular magnetic fields by using the Landauer-Büttiker formula combining with the nonequilibrium Green's-function method. While the Fermi energy just crosses discrete transverse channels, the transmission coefficient of the quantized plateaus jumps from one step to another and the Seebeck coefficient S_c and the thermoelectric figure of merit ZT show

peaks. Due to the electron-hole symmetry, S_c is odd function of the Fermi energy E_F , and ZT is even function. S_c and ZT have very large peaks near the Dirac point at the zero magnetic field and zero gate voltage, because of the extra π Berry phase around the TI nanowire and a gap appearance in the energy spectrum. The thermoelectric properties of the TI nanowire are obviously dependent on the gate voltage and the longitudinal and perpendicular magnetic fields. The values of S_c and ZT can be easily controlled by changing the gate voltage or magnetic fields. In addition, the effect of the disorder on the thermoelectric properties is also studied. The Seebeck coefficient S_c and ZT are robust against the disorder, but the plateaus in the conductance are broken. This is very counterintuitive. In usual, the S_c and ZT are more sensitive than the conductance. In particular, the large peak value of ZT can well survive, which is very promising for the application of the thermoelectricity.

The rest of the paper is organized as follows. In Sec. II, the effective tight-binding Hamiltonian is introduced. The formalisms for calculating the Seebeck coefficient S_c and the thermoelectric figure of merit ZT are then derived. In Sec. III, the thermoelectric properties at zero perpendicular magnetic field and zero gate voltage are studied. Sec. IV and Sec. V contribute to the effect of the perpendicular magnetic field, gate voltage, and disorder on thermoelectric properties, respectively. Finally, a brief summary is drawn in Sec. VI.

II. MODEL AND METHODS

Here we consider a cuboid 3D TI nanowire under the longitudinal and perpendicular magnetic fields as shown in Fig.1(a). Based on the lattice model, the two-dimensional Hamiltonian for surface states of the 3D TI nanowire can be described as follows,⁴⁶

$$H = \sum_m \left[\sum_n^N c_{nm}^\dagger R_0 c_{nm} + \sum_n^N c_{nm}^\dagger R_y c_{n,m+1} + \sum_n^{N-1} c_{nm}^\dagger R_{xn} c_{n+1,m} - c_{Nm}^\dagger R_{xN} c_{1m} + \text{H.c.} \right], \quad (1)$$

with

$$\begin{aligned} R_0 &= (2W/a)\sigma_z + U_n\sigma_0, \\ R_{xn} &= [-(W/2a)\sigma_z + (i\hbar\nu_F/2a)\sigma_y]e^{i(\phi_{n,n+1}^\parallel + \phi_{n,n+1}^\perp)}, \\ R_y &= -(W/2a)\sigma_z - (i\hbar\nu_F/2a)\sigma_x, \end{aligned} \quad (2)$$

where c_{nm} and c_{nm}^\dagger are the annihilation and creation operators at site (n, m) respectively, with the index m being along the y-direction and n being along the circumference of the TI nanowire. N is the total number of lattices encircling the TI nanowire, a is the lattice constant, ν_F is the Fermi velocity, $\sigma_x, \sigma_y, \sigma_z$ are the Pauli matrices, σ_0 is the unit matrix, and U_n is the on-site energy which can be regulated by the gate voltage. Here we set $U_n = \Delta U/2$

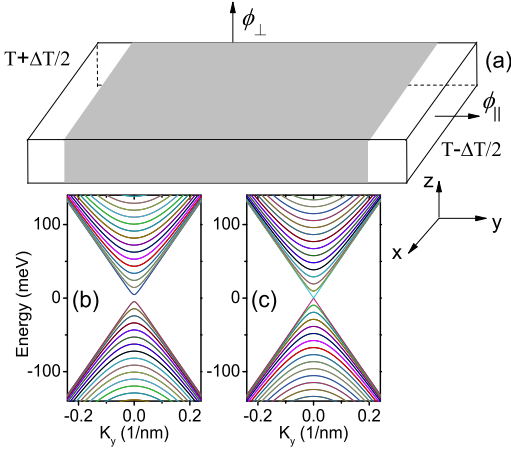


FIG. 1: (a) The schematic of a cuboid 3D TI nanowire under the longitudinal and perpendicular magnetic fields. The grey region is the center scattering region. (b) and (c) show the energy band structure of the TI nanowire with the longitudinal magnetic flux $\phi_{\parallel} = 0$ and π , respectively. The perpendicular magnetic field $\phi_{\perp} = 0$, gate voltage $\Delta U = 0$, and the disorder strength $D = 0$.

for the upper surface, $U_n = -\Delta U/2$ for the lower surface, and U_n is linear from $\Delta U/2$ to $-\Delta U/2$ for two side surfaces. Here the effect of longitudinal magnetic field is included by adding a phase term $\phi_{n,n+1}^{\parallel} = \int_n^{n+1} \mathbf{A}_{\parallel} \cdot d\mathbf{l}/\phi_0$ to R_{xn} in Eq.(2), where $\mathbf{A}_{\parallel} = (0, 0, B_{\parallel}x)$ is the vector potential for a magnetic field B_{\parallel} parallel to the y direction. Furthermore, we also consider a uniform magnetic field B_{\perp} perpendicular to the upper and lower surfaces [see Fig.1(a)], then a phase $\phi_{n,n+1}^{\perp} = \int_n^{n+1} \mathbf{A}_{\perp} \cdot d\mathbf{l}/\phi_0$ is added in the hopping term R_{xn} , where $\mathbf{A}_{\perp} = (B_{\perp}y, 0, 0)$. W in Eq.(2) is the Wilson term. The Wilson term is introduced for solving the fermion doubling problem in the lattice model.⁴⁶ In the numerical calculations, W is set $0.3\hbar\nu_F$. The nanowire is assumed to have a cross section of a size $(L_x, L_z) = (96 \text{ nm}, 12 \text{ nm})$. For the nanowires of other sizes, the results are similar. We also set the Fermi velocity $\nu_F = 5 \times 10^5 \text{ m/s}$ and the lattice constant $a = 0.6 \text{ nm}$.^{11,47}

Considering that the bias and temperature of the left/right terminal are $V_{L/R}$ and $\mathcal{T}_{L/R}$, the electronic current and the electric-thermal current flowing from the left terminal to the cuboid 3D TI nanowire can be calculated from the Landauer-Büttiker formula,²⁶

$$J_L = \frac{e}{h} \int T_{LR}(E) [f_L(E) - f_R(E)] dE, \quad (3)$$

$$Q_L = \frac{1}{h} \int (E - \mu_L) T_{LR}(E) [f_L(E) - f_R(E)] dE.$$

Here, we neglect the heat current carried by the phonon, because that this part of the heat current is usually much smaller than that induced by the electron at low temper-

ature. In Eq.(3),

$$f_{\alpha}(E, \mu_{\alpha}, \mathcal{T}_{\alpha}) = \frac{1}{e^{(E - \mu_{\alpha})/k_B \mathcal{T}_{\alpha}} + 1} \quad (4)$$

is the Fermi distribution function of the left/right terminals, where $\alpha = L$ or R for the left or right terminal, and the chemical potential $\mu_{\alpha} = E_F + eV_{\alpha}$ with the Fermi energy E_F .

$T_{LR}(E)$ in Eq.(3) is the transmission coefficient through the 3D TI nanowire. By using nonequilibrium Green's function method, $T_{LR}(E)$ can be obtained as: $T_{LR}(E) = \text{Tr}[\mathbf{\Gamma}_L \mathbf{G}^r \mathbf{\Gamma}_R \mathbf{G}^a]$, in which $\mathbf{\Gamma}_{L/R}(E) = i[\mathbf{\Sigma}_{L/R}^r(E) - \mathbf{\Sigma}_{L/R}^a(E)]$ and the Green's function $\mathbf{G}^r(E) = [\mathbf{G}^a]^{\dagger} = [E\mathbf{I} - \mathbf{H}^{\text{cen}} - \sum_{\alpha} \mathbf{\Sigma}_{\alpha}^r]^{-1}$, with \mathbf{H}^{cen} being the Hamiltonian of center scattering region and the self-energy $\mathbf{\Sigma}_{L/R}^{r/a}$ stems from coupling to the left/right lead.^{48,49} For a clean TI nanowire, the center scattering region can arbitrarily be taken and the results are exactly identical. On the other hand, while in the presence of disorder,⁵⁰ we consider that the disorder only exist in the center scattering region and the left and right terminals are the perfect semi-infinite 3D TI nanowire still. In the presence of disorder, the on-site energies at the center region are added with a term $D_{nm}\sigma_0$ with

$$D_{nm} = \sum_{n',m'} \tilde{D}_{n'm'} \exp\left(-\frac{r_{nm,n'm'}^2}{2\xi^2}\right). \quad (5)$$

Here $\tilde{D}_{n'm'}$ is uniformly distributed in the interval $[-D/2, D/2]$ with D being the disorder strength, $r_{nm,n'm'}$ is the distance between site (n, m) and (n', m') , and ξ is the parameter describing the correlation length of the disorder. In the numerical calculation, we consider the long range disorder with $\xi = 5a$ and the disorder density 50%. With each value of disorder strength D , the transmission coefficient $T_{LR}(E)$, the conductance, Seebeck coefficient, thermal conductance, and ZT are averaged up to 40 configurations in the calculation.

In the case of very low bias and very small temperature gradient, the Fermi distribution function in Eq.(3) can be expanded linearly in terms of the Fermi energy E_F and the temperature \mathcal{T} as

$$f_{L/R}(E, \mu_{L/R}, \mathcal{T}_{L/R}) = f_0 - eV_{L/R} \frac{\partial f_0}{\partial E} + \Delta \mathcal{T}_{L/R} \frac{\partial f_0}{\partial \mathcal{T}}, \quad (6)$$

where $\Delta \mathcal{T}_{L/R} = \mathcal{T}_{L/R} - \mathcal{T}$ and $f_0 = [e^{(E - E_F)/k_B \mathcal{T}} + 1]^{-1}$ is the Fermi distribution function at the zero thermal gradient and zero bias. Then linear thermoelectric transport can be calculated while a small external bias voltage $\delta V = V_L - V_R$ or/and a small temperature gradient $\delta \mathcal{T} = \mathcal{T}_L - \mathcal{T}_R$ is applied between the left and right terminals.

By introducing the integrals $I_i(\mathcal{T}) = \frac{1}{h} \int dE (E - E_F)^i (-\frac{\partial f_0}{\partial E}) T_{LR}(E)$ ($i = 0, 1, 2$), the linear-electric conductance G ($G = I_L/\delta V$ at the zero thermal gradient),

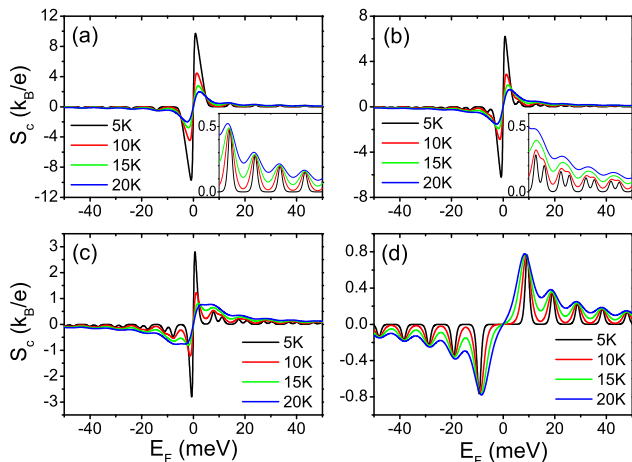


FIG. 2: Panels (a)-(d) plot the Seebeck coefficients S_c versus Fermi energy E_F for different temperatures with the longitudinal magnetic flux $\phi_{\parallel} = 0, \pi/3, 2\pi/3, \text{ and } \pi$, respectively. The insets in panels (a) and (b) are zoom-in figures of the small peaks in the corresponding main figures. The perpendicular magnetic field $\phi_{\perp} = 0$ and gate voltage $\Delta U = 0$.

the Seebeck coefficients S_c ($S_c = \delta V / \delta T$ at the zero electric current I_L case), and electric thermal conductance κ_e ($\kappa_e = Q_L / \delta T$ at the zero electric current) can be expressed in very simple forms^{24,51}

$$G = e^2 I_0(T), \quad (7)$$

$$S_c = -\frac{1}{eT} \frac{I_1(T)}{I_0(T)}, \quad (8)$$

$$\kappa_e = \frac{1}{T} \left[I_2(T) - \frac{I_1^2(T)}{I_0(T)} \right]. \quad (9)$$

After solving G , S_c , and κ_e , the thermoelectric figure of merit $ZT = GS_c^2 T / \kappa_e$ can be obtained straightforwardly.

III. THERMOELECTRIC PROPERTIES AT ZERO PERPENDICULAR MAGNETIC FIELD AND ZERO GATE VOLTAGE

First, we study the Seebeck coefficient S_c and the thermoelectric figure of merit ZT at the zero magnetic field and zero gate voltage. Figure 2(a) and Fig.3(a) show S_c and ZT versus the Fermi energy E_F for different temperatures. Due to electron-hole symmetry, S_c is an odd function of the Fermi energy E_F with $S_c(-E_F) = -S_c(E_F)$. However, ZT is an even function of E_F with $ZT(-E_F) = ZT(E_F)$. The properties $S_c(-E_F) = -S_c(E_F)$ and $ZT(-E_F) = ZT(E_F)$ can remain even if in the presence of the magnetic field, gate voltage, and disorder. S_c and ZT exhibit a series of peaks at low temperatures. When E_F crosses the discrete transverse channels where the transmission coefficient T_{LR} jumps from one integer to another, S_c and ZT

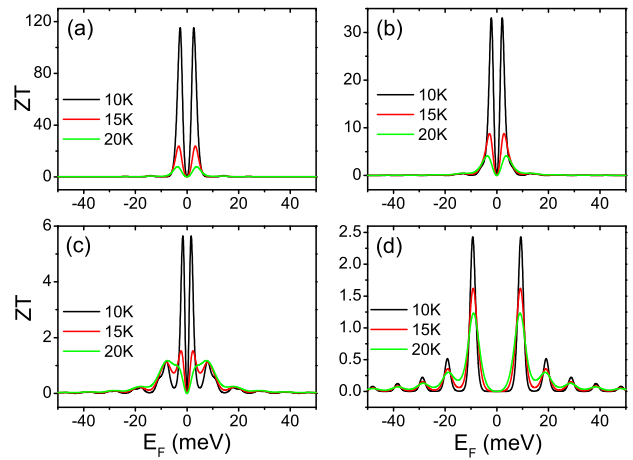


FIG. 3: Panels (a)-(d) plot ZT versus E_F for different temperatures with the longitudinal magnetic flux $\phi_{\parallel} = 0, \pi/3, 2\pi/3, \text{ and } \pi$, respectively. The perpendicular magnetic field $\phi_{\perp} = 0$ and gate voltage $\Delta U = 0$.

show peak. The closer the Dirac point is, the higher the peak is. S_c and ZT have the highest peak near the Dirac point. The value of ZT at the highest peak exceeds over 100 at the temperature $T = 10K$. The highest peak is much higher than other peaks. For S_c (ZT), the highest peak is about 10 (100) times higher than the second highest peak. This is because of the π Berry phase around the 3D TI nanowire and the wormhole effect, and an energy gap opens at the zero magnetic field at the Dirac point, leading that the transmission coefficient $T_{LR} = 0$. In order to balance the thermal forces acting on the charge carriers, it needs a very large bias which results in a very large S_c and ZT near the Dirac point. When the temperature rises, the height of the highest peak of S_c decreases, but the heights of the other peaks roughly remain unchanged and the valleys rise.

Next, we study the effect of the longitudinal magnetic field B_{\parallel} on the Seebeck coefficient S_c and the thermoelectric figure of merit ZT . Here the longitudinal magnetic field is described by the magnetic flux Φ_{\parallel} in the cross section of the TI nanowire, with $\Phi_{\parallel} = L_x L_y B_{\parallel}$. Figure 1(b) and 1(c) show the energy band structures of the TI nanowire at $\phi_{\parallel} \equiv \Phi_{\parallel} / \phi_0 = 0$ and π . Because of a π Berry phase for electron going around the four facets of TI nanowire,¹³⁻¹⁵ it yields a gapped spectrum of surface state at $\phi_{\parallel} = 0$. At $\phi_{\parallel} = 0$, each band is double degenerate. With the increase of ϕ_{\parallel} from zero, the Aharonov-Bohm phase emerges and the double degeneracy is removed.¹⁸⁻²⁰ One sub-band moves up and other sub-band goes down, leading that the gap becomes narrower. When the magnetic flux $\phi_{\parallel} = \pi$, the π Aharonov-Bohm phase exactly cancels the π Berry phase, leading that a pair of non-degenerate linear modes emerge with the gap closing [Fig.1(c)]. But other bands are double degenerate again. Now it is ready to study the effect of the longitudinal magnetic field ϕ_{\parallel} on the thermoelectric properties. S_c and ZT are the periodic functions of ϕ_{\parallel}

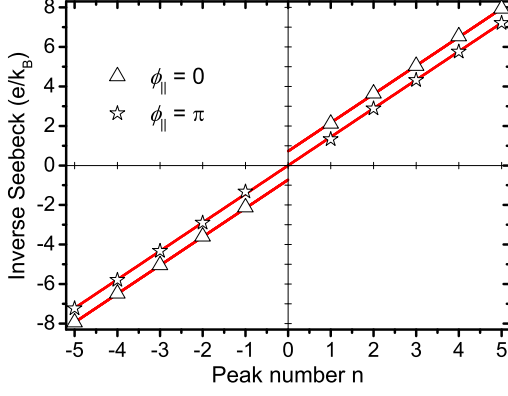


FIG. 4: The inverse of peak height of Seebeck coefficients S_c vs the peak number n . The upper triangle symbol and hollow pentagram symbol denote the magnetic flux $\phi_{\parallel} = 0$ and π . These data points are obtained from the curve of $T = 5K$ in Fig.2(a) and 2(d). The two red lines are $\frac{e}{k_B}(n + \text{sign}(n)/2)/\ln 2$ and $\frac{e}{k_B}n/\ln 2$.

with $S_c(\phi_{\parallel}) = S_c(\phi_{\parallel} + 2\pi)$ and $ZT(\phi_{\parallel}) = ZT(\phi_{\parallel} + 2\pi)$. In addition, $S_c(\phi_{\parallel}) = S_c(-\phi_{\parallel})$ and $ZT(\phi_{\parallel}) = ZT(-\phi_{\parallel})$ because that the system is invariant by simultaneously making the time-inversion transformation and rotation 180° by fixing the x axis. In Fig.2 and Fig.3, we show the Seebeck coefficient S_c and the thermoelectric figure of merit ZT for the longitudinal magnetic flux $\phi_{\parallel} = 0, \pi/3, 2\pi/3, \text{ and } \pi$, respectively. When ϕ_{\parallel} increases from zero, all peaks in the curves of $S_c \sim E_F$ and $ZT \sim E_F$ split into two due to that the double degeneracy is removed. The height of the highest peak near the Dirac point also gradually decrease. Especially for ZT , the trend of decreasing is very obvious. But the value ZT is still over 30 at $\phi_{\parallel} = \pi/3$. For $\phi_{\parallel} = \pi$, the highest peak near the Dirac point disappear completely because of the close of the energy gap. But other peaks can remain still, and two adjacent peaks combine into a single peak again. In this case, S_c and ZT are small. Therefore, the thermoelectric properties (S_c and ZT) can be well adjusted by the longitudinal magnetic field. In fact, for $\phi_{\parallel} = \pi$, the magnetic field B_{\parallel} is about 11.3 Tesla.

Figure 4 shows the inverse of the peak height of Seebeck coefficient S_c versus the peak number n with the longitudinal magnetic flux $\phi_{\parallel} = 0$ and π . Here the peak number n denotes the n -th peak near the Dirac point, but the highest peak does not count at $\phi_{\parallel} = 0$. In fact, except for the highest peak, the heights of the other peaks are almost independent of temperature [see Fig.2(a) and 2(d)]. We can see that at $\phi_{\parallel} = 0$ the inverse of the peak height is proportional to $\frac{e}{k_B}(n + \text{sign}(n)/2)/\ln 2$ with $\text{sign}(n) = 1$ for $n > 0$ and -1 for $n < 0$ (see the upper triangle symbol in Fig.4). This is similar as that in the conventional metal.²⁵ On the other hand, for $\phi_{\parallel} = \pi$, the inverse of the peak height is proportional to $\frac{e}{k_B}n/\ln 2$ (see the hollow pentagram symbol in Fig.4), which is similar as that in graphene.²⁵ This is because that the extra π Berry

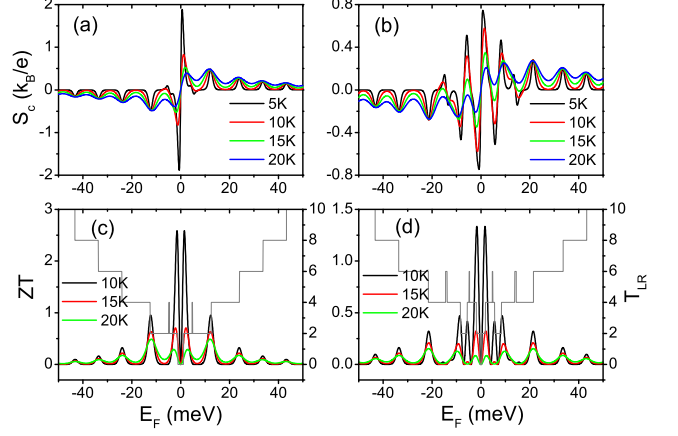


FIG. 5: The Seebeck coefficient S_c and ZT vs Fermi energy E_F for different temperatures. $\phi_{\parallel} = 0, \phi_{\perp} = 0$, and the gate voltage $\Delta U = 30\text{meV}$ in panels (a) and (c) and $\Delta U = 50\text{meV}$ in panels (b) and (d). The gray curves in (c) and (d) are the transmission coefficient T_{LR} .

phase and the wormhole effect lead to a half-integer shift in the curve of the inverse of the peak height of S_c versus the peak number n . In fact, these conclusions can also analytically be obtained from the energy band structure and the transmission coefficient $T_{LR}(E)$. Taking $\phi_{\parallel} = 0$ with the positive n as an example, when the energy E is in the vicinity of E_n , the transmission coefficient $T_{LR}(E)$ can be written as $T_{LR}(E) = 2n$ at $E < E_n$ and it jumps to $2n+2$ at $E > E_n$ with E_n being the bottom of the n -th sub-band. Then substituting this transmission coefficient $T_{LR}(E)$ into Eq.(8), we can obtain

$$S_c(E_F) = \frac{k_B}{e} \frac{-xe^x + (1+e^x)\ln(1+e^x)}{1+n(1+e^x)}, \quad (10)$$

with $x \equiv (E_n - E_F)/k_B T$. This equation gives the shape of the n -th peak for $\phi_{\parallel} = 0$ with the positive n . So the height of the n -th peak of S_c is about $\frac{k_B}{e} \ln 2 / (n + 1/2)$. From $S_c(-E_F) = -S_c(E_F)$, the peak heights for the negative n can be obtained as $\frac{k_B}{e} \ln 2 / (n - 1/2)$ straightforwardly. Similarly, the shape of the n -th peak of S_c for $\phi_{\parallel} = \pi$ can analytically be derived

$$S_c(E_F) = \frac{k_B}{e} \frac{-xe^x + (1+e^x)\ln(1+e^x)}{1+(n-1/2)(1+e^x)}, \quad (11)$$

and the peak height is $\frac{k_B}{e} \ln 2 / n$. In Fig.4, the curves $\frac{e}{k_B}(n + \text{sign}(n)/2)/\ln 2$ and $\frac{e}{k_B}n/\ln 2$ (the analytic results for the inverse of the peak height of S_c) are also shown. They are well consistent with the numerical points.

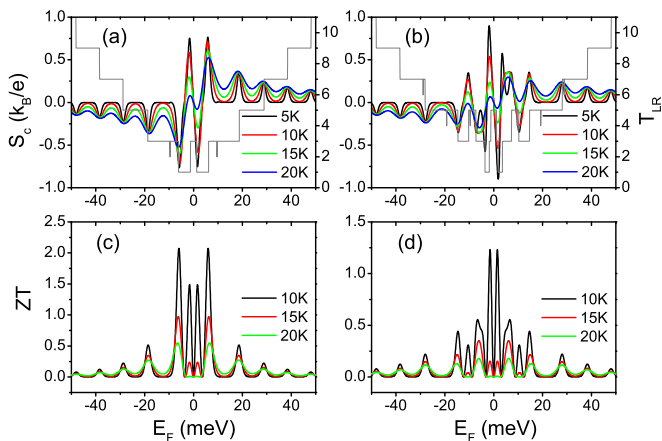


FIG. 6: S_c and ZT vs Fermi energy E_F for different temperatures. $\phi_{\parallel} = \pi$, $\phi_{\perp} = 0$, and the gate voltage $\Delta U = 30\text{meV}$ in panels (a) and (c) and $\Delta U = 50\text{meV}$ in panels (b) and (d). The gray curves in (a) and (b) are the transmission coefficient T_{LR} .

IV. EFFECT OF THE PERPENDICULAR MAGNETIC FIELD AND GATE VOLTAGE ON THERMOELECTRIC PROPERTIES

In this section, we study the effect of the perpendicular magnetic field B_{\perp} and gate voltage ΔU on the Seebeck coefficient S_c and thermoelectrical figure of merit ZT of the 3D TI nanowire. First, the effect of ΔU is studied. Figure 5 shows S_c and ZT with $\phi_{\parallel} = 0$, and the gate voltage ΔU being 30meV and 50meV . The parameters in Fig.6 are similar to Fig.5, but $\phi_{\parallel} = \pi$. In order to explain the behavior of S_c and ZT clearly, the transmission coefficient T_{LR} is also given in Fig.5 and Fig.6, and here T_{LR} is quantized and exhibits a series of plateaus. In Fig.5, in which the longitudinal magnetic flux $\phi_{\parallel} = 0$, we see that S_c and ZT show peaks when T_{LR} jumps from one step to another. In particular, as the gate voltage increases, the large ZT at $\Delta U = 0$ [see Fig.3(a)] reduces swiftly. When $\Delta U = 20\text{meV}$, the value of ZT is about 15.6. So the gate voltage can regulate the thermoelectric properties. In addition, the oscillation peak near the Dirac point becomes dense in the presence of ΔU [see Fig.5(b) and (d)]. Because that the gate voltage ΔU causes the difference between the potential energies of the upper and lower surfaces, it affects the states of the side surfaces, and makes the energy band deform, which leads to a strong reduction of the energy gap. Figure 6 shows the curve of $S_c \sim E_F$ and $ZT \sim E_F$ at the longitudinal magnetic flux $\phi_{\parallel} = \pi$. Similarly, S_c and ZT display peaks when the transmission coefficient T_{LR} steps jump. The dense peaks are also displayed near Dirac point when the gate voltage ΔU increases. By comparing between Fig.5(b,d) and Fig.6(b,d), for $\Delta U = 50\text{meV}$, we find that the curves of $S_c \sim E_F$ and $ZT \sim E_F$ are very similar, although $\phi_{\parallel} = 0$ in Fig.5 and $\phi_{\parallel} = \pi$ in Fig.6. This means that both the π Berry phase and the Aharonov-Bohm

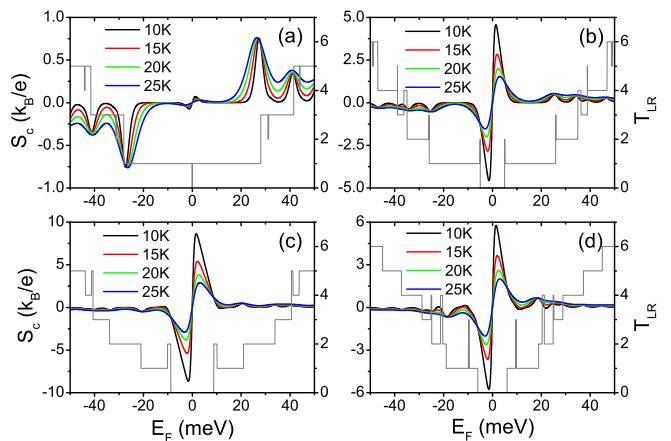


FIG. 7: The Seebeck coefficient S_c vs E_F for different temperatures with the perpendicular magnetic field $\phi_{\perp} = 0.005$ and $\phi_{\parallel} = 0$. The gate voltage $\Delta U = 0\text{meV}$ (a), 10meV (b), 20meV (c), and 50meV (d). The gray curves in (a-d) are the transmission coefficient T_{LR} .

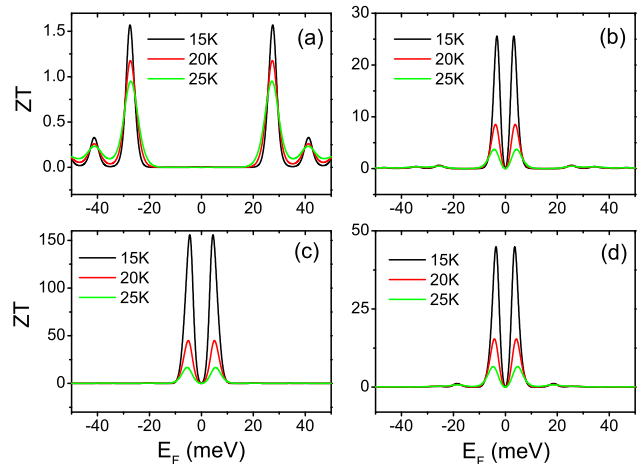


FIG. 8: ZT vs E_F for different temperatures with $\phi_{\perp} = 0.005$ and $\phi_{\parallel} = 0$. The gate voltage $\Delta U = 0\text{meV}$ (a), 10meV (b), 20meV (c), and 50meV (d).

phase of ϕ_{\parallel} have little effect on the Seebeck coefficient S_c and ZT while at the large gate voltage.

Now, we study the effect of the perpendicular magnetic field B_{\perp} on the Seebeck coefficient S_c and the thermoelectric figure of merit ZT . For the small B_{\perp} (e.g. $B_{\perp} < 0.1$ Tesla), S_c and ZT are almost unaffected, and ZT has still large value at $\phi_{\parallel} = 0$. On the other hand, for a large perpendicular magnetic field B_{\perp} , Landau levels form and edge states appear on the side surfaces. In this case, S_c and ZT are almost independent of the longitudinal magnetic field ϕ_{\parallel} and ZT strongly reduces. Figure 7(a) and Fig.8(a) show S_c and ZT versus the Fermi energy E_F with the perpendicular magnetic flux in a lattice $\phi_{\perp} = 0.005$ (the real magnetic field B_{\perp} is around 18.3 Tesla). The S_c displays peaks when E_F passes the Landau levels and show valleys between adja-

cent Landau levels. Because that the Landau levels are highly degenerate, the number of energy levels decreases, and as a result the peak spacing becomes larger and the peak becomes sparse. When E_F is on the zeroth Landau level, S_c is zero. This is because the zeroth Landau level with the doubly degeneracy is shared equally by electrons and holes, and the electrons and holes give the opposite contributions to S_c . Moreover, the peak height of S_c is proportional to $\frac{k_B}{e} \ln 2/n$ with the peak number n . With the increase of temperature \mathcal{T} , the peak height of S_c remains approximately unchanged, but the valley rises, which shows that S_c peaks are robust against the temperature. For the thermoelectric figure of merit ZT , it is small for all the Fermi energy E_F , because of the appearance of the edge states and the absence of the energy gap at the large ϕ_\perp . In addition, there are two largest peaks in ZT at $E_F \approx \pm 27.3\text{meV}$ (27.3meV is the first Landau level). The positions of the ZT peaks are corresponding to the S_c peaks. With the increase of ϕ_\perp , the peak spacing of ZT becomes larger and the peak becomes sparse similar to the peaks of S_c .

Let us study the case of the coexistence of both the perpendicular magnetic field ϕ_\perp and gate voltage ΔU . Figure 7(b-d) and Fig.8(b-d) show S_c and ZT at the large ϕ_\perp ($\phi_\perp = 0.005$) and zero ϕ_\parallel for the different ΔU . For the large ϕ_\perp , the Landau levels form, and both S_c and ZT are almost independent of the longitudinal magnetic flux ϕ_\parallel . When the gate voltage ΔU is applied, the Landau levels of the upper and lower surfaces split, and then it produces a gap spectrum of surface states in the TI nanowire. So the highest peaks of S_c and ZT near the Dirac point appear, and the value of ZT strongly increases. While $\Delta U \geq 10\text{meV}$, ZT can exceed over 25. In addition, we can see from Fig.7 and Fig.8 that when the gate voltage increases, the bandgap of surface states increases first and then decreases due to the side surfaces. So the highest peak of S_c and ZT also tends to increase first and then decrease. But ZT can remain the large value in a very large range of ΔU . In short, by adjusting the longitudinal, perpendicular magnetic fields and gate voltage, it is easy to change the value of S_c and ZT greatly, i.e. to change greatly the thermoelectric properties of the 3D TI nanowire.

V. EFFECT OF THE DISORDER ON THERMOELECTRIC PROPERTIES

Up to now, we have shown that the Seebeck coefficient S_c and the thermoelectric figure of merit ZT have the large value at zero magnetic fields with the zero gate voltage, or at the large perpendicular magnetic field with the nonzero gate voltage. Next, let us study the effect of the disorder on S_c and ZT . Figure 9 shows the transmission coefficient T_{LR} , S_c and ZT for the different disorder strength D at the zero perpendicular magnetic field. When the disorder strength $D = 0$, T_{LR} displays quantum plateaus. While in the presence of the disorder

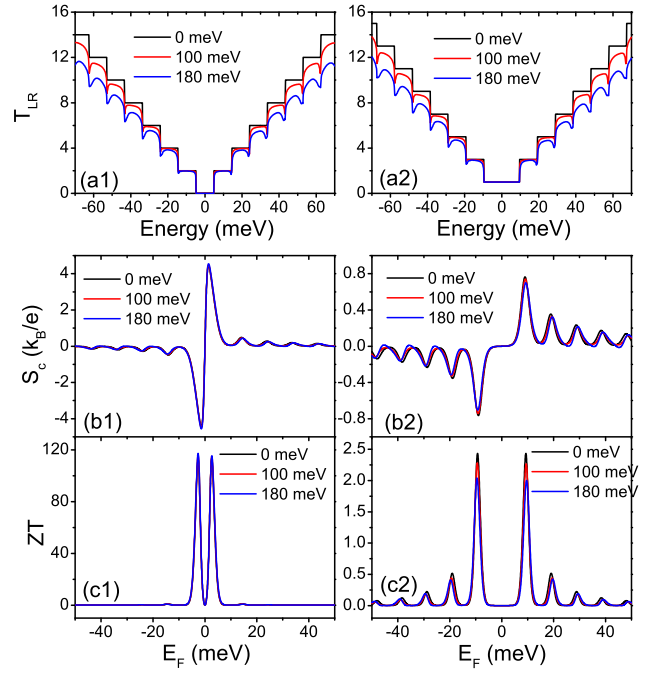


FIG. 9: The transmission coefficient T_{LR} vs the energy E (a), the Seebeck coefficient S_c vs E_F (b) and ZT vs E_F (c) for the different disorder strengths D . The temperature $\mathcal{T} = 10\text{K}$, the gate voltage $\Delta U = 0$ meV, $\phi_\perp = 0$, and $\phi_\parallel = 0$ for panels (a1)-(c1) and π for panels (a2)-(c2).

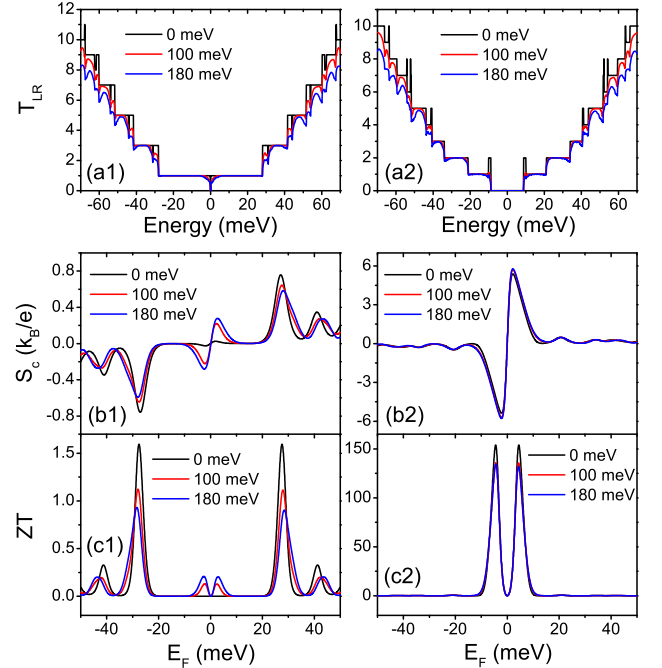


FIG. 10: T_{LR} vs energy E (a), S_c vs E_F (b) and ZT vs E_F (c) for the different disorder strengths D . The perpendicular magnetic field $\phi_\perp = 0.005$, the longitudinal magnetic field $\phi_\parallel = 0$, the temperature $\mathcal{T} = 15\text{K}$, and the gate voltage $\Delta U = 0\text{meV}$ for the panels (a1)-(c1) and 20 meV for the panels (a2)-(c2).

der ($D \neq 0$), the lower plateaus (e.g. the plateaus with $T_{LR} = 0$ and 1) are robust against disorder. On the other hand, the higher plateaus of T_{LR} are obviously destroyed, because that the scattering occurs by the disorders. But the results show that S_c and ZT are very robust against disorder in a wide range of Fermi energy E_F . Not only the highest peak near Dirac point can survive, but also the low peak at large E_F can remain at the strong disorder. Even the disorder strength $D = 180\text{meV}$, the peak value of ZT can still exceed over 100 [see Fig.9(c1)] and these lower peaks remain almost the same [see Fig.9(b1), (b2) and (c2)]. This is obviously different from the intuition, because thermoelectric behaviors (S_c and ZT) are more sensitive to the density of state than the conductance (or transmission coefficient). In fact, although the plateaus of T_{LR} are obviously destroyed by the disorder, the sudden jumps from one plateau to another still exist and the position of the jump point remains unchanged. Because the peaks of S_c and ZT are mainly determined by the jumps of T_{LR} , they are robust against the disorder. The characteristics of ZT having the large value and being robust against the disorder are beneficial for the application of the thermoelectricity.

Figure 10 shows the transmission coefficient T_{LR} , S_c and ZT for the different disorder strength at the high perpendicular magnetic field $\phi_{\perp} = 0.005$ with the gate voltage $\Delta U = 0$ and 20meV . While $\Delta U = 0$, S_c and ZT are small for the clean TI nanowire. The disorder reduce the heights of the peaks of S_c and ZT , and slightly shifts the peak positions also. For example, while the disorder strength $D = 180\text{meV}$, the peak heights of ZT decrease to about half of that at $D = 0$. On the other hand, for the case with the non-zero gate voltage (e.g. $\Delta U = 20\text{meV}$), S_c and ZT have the large peak values while the disorder strength $D = 0$. With the increasing of D , the peak heights and positions of S_c and ZT can remain unchanged almost. When $D = 180\text{meV}$, the largest value of ZT can still exceed over 100. ZT not only has a large value, but also is robust against the disorder, which is very promising for the application.

VI. CONCLUSIONS

In summary, we study the magnetothermoelectric transport properties of the surface states of 3D TI

nanowires under the longitudinal and perpendicular magnetic fields. The Seebeck coefficient S_c and the thermoelectric figure of merit ZT show peaks where there are step changes of transmission coefficient. Due to the electron-hole symmetry, the Seebeck coefficient is odd function of the Fermi energy E_F , and ZT is even function. The highest peak appears when E_F is near the Dirac point, and the peak heights gradually decrease with E_F far from the Dirac point. At the zero magnetic field and zero gate voltage, the Seebeck coefficient and ZT have the large peak value due to the π Berry phase around the topological insulator nanowire and the wormhole effect. The Seebeck coefficient S_c and ZT are obviously dependent on the gate voltage, the longitudinal, and perpendicular magnetic fields. This means that the thermoelectric properties of the 3D TI nanowire can be easily adjusted by tuning the gate voltage or magnetic fields. At zero magnetic fields and zero gate voltage, or at the large perpendicular magnetic field and nonzero gate voltage, ZT has the large value. In addition, the effect of the disorder on the thermoelectric properties is also studied. It is a surprise that the Seebeck coefficient and ZT are more undisturbed than the conductance (transmission coefficient). The plateaus of transmission coefficient can be broken by the disorder, but the peaks at the Seebeck coefficient and ZT are robust against the disorder, because the jumps of transmission coefficient can remain in the presence of the disorder. The characteristics, that ZT has the large value and is robust against the disorder, are very beneficial for the application of the thermoelectricity.

Acknowledgement

This work was financially supported by National Key R and D Program of China (2017YFA0303301), NBRP of China (2015CB921102), NSF-China (Grants No. 11574007), and the Key Research Program of the Chinese Academy of Sciences (Grant No. XDPB08-4).

* sunqf@pku.edu.cn

¹ C.L. Kane and E.J. Mele, Phys. Rev. Lett. **95**, 226801 (2005).

² B.A. Bernevig, T.L. Hughes, and S.-C. Zhang, Science **314**, 1757 (2006).

³ M. König, S. Wiedmann, C. Brüne, A. Roth, H. Buhmann, L.W. Molenkamp, X.-L. Qi, and S.-C. Zhang, Science **318**, 766 (2007).

⁴ M.Z. Hasan and C.L. Kane, Rev. Mod. Phys. **82**, 3045

(2010).

⁵ X.-L. Qi and S.-C. Zhang, Rev. Mod. Phys. **83**, 1057 (2011).

⁶ H. Zhang, C.-X. Liu, X.-L. Qi, X. Dai, Z. Fang, and S.-C. Zhang, Nat. Phys. **5**, 438 (2009).

⁷ Y.L. Chen, J.G. Analytis, J.-H. Chu, Z.K. Liu, S.-K. Mo, X.L. Qi, H.J. Zhang, D.H. Lu, X. Dai, Z. Fang, S.C. Zhang, I.R. Fisher, Z. Hussain, and Z.-X. Shen, Science **325**, 178 (2009).

- ⁸ Y. Xia, D. Qian, D. Hsieh, L. Wray, A. Pal, H. Lin, A. Bansil, D. Grauer, Y.S. Hor, R.J. Cava, and M.Z. Hasan, *Nat. Phys.* **5**, 398 (2009).
- ⁹ D. Hsieh, Y. Xia, L. Wray, D. Qian, A. Pal, J.H. Dil, J. Osterwalder, F. Meier, G. Bihlmayer, C.L. Kane, Y.S. Hor, R.J. Cava, and M.Z. Hasan, *Science* **323**, 919(2009).
- ¹⁰ Y. Xu, I. Miotkowski, C. Liu, J. Tian, H. Nam, N. Alidoust, J. Hu, C.-K. Shih, M.Z. Hasan, and Y.P. Chen, *Nat. Phys.* **10**, 956 (2014); Y. Xu, I. Miotkowski, and Y.P. Chen, *Nat. Commun.* **7**, 11434 (2016).
- ¹¹ R. Yoshimi, A. Tsukazaki, Y. Kozuka, J. Falson, K.S. Takahashi, J.G. Checkelsky, N. Nagaosa, M. Kawasaki, and Y. Tokura, *Nat. Commun.* **6**, 6627 (2015).
- ¹² N. Koirala, M. Brahlek, M. Salehi, L. Wu, J. Dai, J. Waugh, T. Nummy, M.-G. Han, J. Moon, Y. Zhu, D. Dessau, W. Wu, N.P. Armitage, and S. Oh, *Nano Lett.* **15**, 8245 (2015).
- ¹³ J.H. Bardarson, P.W. Brouwer, and J.E. Moore, *Phys. Rev. Lett.* **105**, 156803 (2010).
- ¹⁴ R. Egger, A. Zazunov, and A.L. Yeyati, *Phys. Rev. Lett.* **105**, 136403 (2010).
- ¹⁵ Y. Zhang and A. Vishwanath, *Phys. Rev. Lett.* **105**, 206601 (2010).
- ¹⁶ H. Peng, K. Lai, D. Kong, S. Meister, Y. Chen, X.-L. Qi, S.-C. Zhang, Z.-X. Shen, and Y. Cui, *Nat. Mater.* **9**, 225 (2010).
- ¹⁷ F. Xiu, L. He, Y. Wang, L. Cheng, L.-T. Chang, M. Lang, G. Huang, X. Kou, Y. Zhou, X. Jiang, Z. Chen, J. Zou, A. Shailos, and K.L. Wang, *Nat. Nanotechnol.* **6**, 216 (2011).
- ¹⁸ J. Dufouleur, L. Veyrat, A. Teichgräber, S. Neuhaus, C. Nowka, S. Hampel, J. Cayssol, J. Schumann, B. Eichler, O.G. Schmidt, B. Büchner, and R. Giraud, *Phys. Rev. Lett.* **110**, 186806 (2013).
- ¹⁹ S.S. Hong, Y. Zhang, J.J. Cha, X.-L. Qi, and Y. Cui, *Nano Lett.* **14**, 2815 (2014).
- ²⁰ S. Cho, B. Dellabetta, R. Zhong, J. Schneeloch, T. Liu, G. Gu, M.J. Gilbert, and N. Mason, *Nat. Commun.* **6**, 7634 (2015).
- ²¹ L. Müchler, F. Casper, B. Yan, S. Chadov, and C. Felser, *Phys. Status Solidi RRL* **7**, 91 (2013).
- ²² N. Xu, Y. Xu, and J. Zhu, *npj Quantum Materials* **2**, 51 (2017).
- ²³ J. He, and Terry M. Tritt, *Science* **357**, 1369 (2017).
- ²⁴ J. Liu, Q.-F. Sun, and X.C. Xie, *Phys. Rev. B* **81**, 245323 (2010).
- ²⁵ Y. Xing, Q.-F. Sun, and J. Wang, *Phys. Rev. B* **80**, 235411 (2009).
- ²⁶ M.M. Wei, Y.T. Zhang, A.M. Guo, J.J Liu, Y. Xing, and Q.-F. Sun, *Phys. Rev. B* **93**, 245432 (2016).
- ²⁷ M. Cutler and N.F. Mott, *Phys. Rev.* **181**, 1336 (1969).
- ²⁸ G. Jeffrey Snyder and E. S. Toberer, *Nat. Mater.* **7**, 105 (2008).
- ²⁹ A.A. Abrikosov, *Fundamentals of the Theory of Metals* (North Holland, Amsterdam, 1988); D.K.C. Macdonald, *Thermoelectricity* (Dover, New York, 2006).
- ³⁰ C.W.J. Beenakker and A.A.M. Staring, *Phys. Rev. B* **46**, 9667 (1992).
- ³¹ S.-G. Cheng, Y. Xing, Q.-F. Sun, and X.C. Xie, *Phys. Rev. B* **78**, 045302 (2008).
- ³² Y. Zhang, J. Song, and Y.-X. Li, *J. Appl. Phys* **117**, 124301 (2015).
- ³³ H.B. Callen, *Phys. Rev.* **73**, 1349 (1948); *Phys. Rev.* **85**, 16 (1952).
- ³⁴ B. Kubala, J. König, and J. Pekola, *Phys. Rev. Lett.* **100**, 066801 (2008).
- ³⁵ L.D. Hicks and M.S. Dresselhaus, *Phys. Rev. B* **47**, 16631 (1993).
- ³⁶ T. Miyasato, N. Abe, T. Fujii, A. Asamitsu, S. Onoda, Y. Onose, N. Nagaosa, and Y. Tokura, *Phys. Rev. Lett.* **99**, 086602 (2007).
- ³⁷ S. Onoda, N. Sugimoto, and N. Nagaosa, *Phys. Rev. B* **77**, 165103 (2008);
- ³⁸ R. Ma, L. Sheng, M. Liu, and D.N. Sheng, *Phys. Rev. B* **87**, 115304 (2013).
- ³⁹ Y. Xu, Z. Gan and S.-C. Zhang, *Phys. Rev. Lett.* **112**, 226801 (2014).
- ⁴⁰ J. Zhang, X. Feng, Y. Xu, M. Guo, Z. Zhang, Y. Ou, Y. Feng, K. Li, H. Zhang, L. Wang, X. Chen, Z. Gan, S.-C. Zhang, K. He, X. Ma, Q.-K. Xue, and Y. Wang, *Phys. Rev. B* **91**, 075431 (2015).
- ⁴¹ B.Z. Rameshti and R. Asgari, *Phys. Rev. B* **94**, 205401 (2016).
- ⁴² J.-W. Li, B. Wang, Y.-J. Yu, Y.-D. Wei, Z.-Z. Yu, and Y. Wang, *Front. Phys.* **12**, 126501 (2017).
- ⁴³ S.Y. Matsushita, K.K. Huynh, H. Yoshino, N.H. Tu, Y. Tanabe, and K. Tanigaki, *Phys. Rev. Materials* **1**, 054202 (2017).
- ⁴⁴ D.S. Shapiro, D.E. Feldman, A.D. Mirlin, and A. Shnirman, *Phys. Rev. B* **95**, 195425 (2017).
- ⁴⁵ M.-S. Lim and S.-H. Jhi, *Solid State Communications* **270**, 22 (2018).
- ⁴⁶ Y.-F. Zhou, H. Jiang, X.C. Xie, and Q.-F. Sun, *Phys. Rev. B* **95**, 245137 (2017).
- ⁴⁷ T. Zhang, P. Cheng, X. Chen, J.-F. Jia, X. Ma, K. He, L. Wang, H. Zhang, X. Dai, Z. Fang, X. Xie, and Q.-K. Xue, *Phys. Rev. Lett.* **103**, 266803 (2009).
- ⁴⁸ W. Long, Q.-F. Sun, and J. Wang, *Phys. Rev. Lett.* **101**, 166806 (2008).
- ⁴⁹ D.H. Lee and J.D. Joannopoulos, *Phys. Rev. B* **23**, 4997 (1981).
- ⁵⁰ S. Cheng, J. Zhou, H. Jiang, and Q.-F. Sun, *New Journal of Physics* **18**, 103024 (2016).
- ⁵¹ T.A. Costi and V. Zlatic, *Phys. Rev. B* **81**, 235127 (2010).